2009-01-0680

Parameterization and Simulation for a Turbocharged Spark Ignition Direct Injection Engine with Variable Valve Timing

Li Jiang, Julien Vanier and Hakan Yilmaz
Robert Bosch LLC

Anna Stefanopoulou
University of Michigan

ABSTRACT

In recent years, advanced automotive technologies have been developed to increase engine output power and improve fuel economy. In order to design dedicated control algorithms for these cutting-edge techniques, a control-oriented model is developed in this paper to capture the behavior of a turbocharged Spark Ignition Direct Injection (SIDI) engine with Variable Valve Timing (VVT). In the proposed model, mean value models are employed to simulate the cycle-average dynamics of the airflow system, while a discrete-event model is used to capture the reciprocating engine combustion cycle. This model, established in Simulink, has been parameterized using experimental data that are collected from a four-cylinder SIDI engine over a wide range of operation conditions. The dynamic performance of this model was validated with data collected during engine transients. In order to explore its modeling capability for flex-fuel applications, the performance of the model with gasoline-ethanol fuel E85 was also investigate.

INTRODUCTION

In order to achieve higher fuel economy with no or minimum penalty in vehicle drivability, various advanced automotive techniques such as Direct Injection (DI), variable valve timing, and turbocharging have received great attention in recent years. At the same time, driven by the ever-rising price of fossil fuels, these technologies have been used to explore the potential of alternative fuel sources, and eventually to develop a vehicle system that can be powered by these fuels with preserved performance. To develop dedicated control algorithm for these cutting-edge techniques, a control-oriented model has been developed in this paper for a turbocharged Spark Ignition Direct Injection (SIDI) engine with Variable Valve Timing (VVT). The development of such a model enables the investigation of the dynamic engine behavior as well as the design of control algorithms.

In the remainder of this paper, existing literature on the modeling of turbocharger, variable valve timing, and engine cyclic performance is first reviewed in each sub-section. Based on these proposed models, an engine model is then developed by systematically integrating the various components to simulate the engine performance with ethanol fuels and investigate the effects of variable valve timing and boost control via wastegate.

In the proposed engine model, a simplified discrete-event mean-value model is used to capture the behavior in an engine combustion cycle and the effects of variable valve timing. For the airflow system, mean-value sub-models are developed for the turbocharger, the throttle, the intercooler, back-pressure drop in the exhaust system, and the filling dynamics in the manifolds. In addition, a mean-value model for the high-pressure fuel injector is also presented. Following the principles of mass and enthalpy conservation, an engine model can then be established by linking these sub-models. The component sub-models are parameterized using the cycle-average experimental data that are collected from a four cylinder SIDI VVT engine over a wide range of operation conditions. The engine model, implemented in Simulink, has finally been validated using experimental

The Engineering Meetings Board has approved this paper for publication. It has successfully completed SAE's peer review process under the supervision of the session organizer. This process requires a minimum of three (3) reviews by industry experts.

ISSN 0148-7191

SAE Customer Service: Tel: 877-606-7323 (inside USA and Canada)
Tel: 724-776-4970 (outside USA)
Fax: 724-776-0790
Email: CustomerService@sae.org
SAE Web Address: http://www.sae.org

Printed in USA

9-2009-01-0680

SAE International

data collected during the engine transients of step changes in throttle angle. In order to evaluate the model performance for flex-fuel applications, the model was also used to predict the behavior of an engine with fuel E85 in the one of the two simulation cases.

MODELING

A control-oriented model is presented in this section for a SIDI VVT engine. Without considering the spatially varying effects, a phenomenological approach is used to develop a lumped-parameter description for the cycle-average behavior of the engine system. In addition, the ordinary differential equations are employed to describe the dynamics in the manifolds and turbocharger. Given the reciprocating combustion behavior of the engine, a discrete-event mean-value model is presented for its stroke-specific dynamics during the intake, compression, combustion, expansion and exhaust blow-down.

As illustrated in Figure 1, ambient air enters the system and a hot-film mass flow sensor measures the intake air flow rate. Next, the air passes through the compressor side of the turbocharger and then the intercooler, which results in a boost pressure that is higher than the ambient pressure. After the air passes through the throttle, it accumulates in the intake manifold and enters the cylinder when the intake valve opens. Depending on the intake and exhaust valve timing, a fraction of the exhaust gas from the current cycle remains in the cylinders and influences the combustion behavior during the next cycle. In the mean time, the injectors spray a demanded amount of fuel directly into the combustion chamber by controlling the fuel rail pressure and injection duration. On the exhaust side, part of the exhaust gas exits via the turbine and generates the power to drive the compressor, while the rest of it passes through the wastegate. The exhaust gas finally returns back to the environment after being treated in the catalyst.

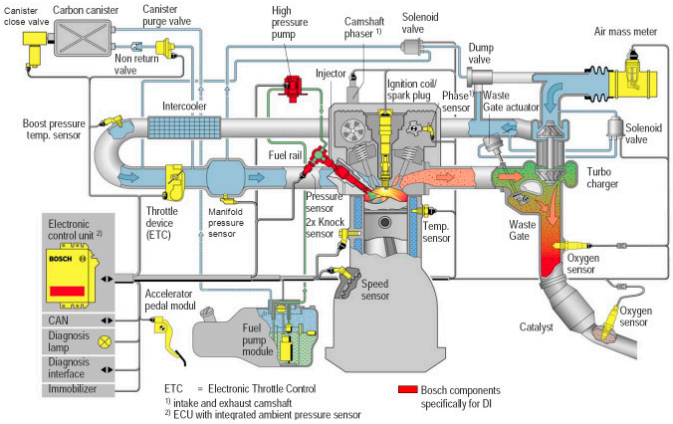

Figure 1: Configuration of a turbocharged direct injection spark ignition engine with variable valve timing

ENGINE

Similar to the model proposed in [1, 2], a discrete-event mean-value model is used to capture the engine behavior during (1) intake valve closing to combustion, (2) instantaneous combustion heat release, (3) polytropic expansion, and (4) exhaust blowdown.

Intake Valve Closing to Start of Combustion

With the residual mass fraction, x_{rg}, estimated from the model for variable valve timing, the mass flow rate of fresh charge drawn from the intake port, W_{fc}, and the residual gas re-breathed from the exhaust port, W_{rg}, can be determined by

$$\begin{aligned} W_{fc} &= n_{cyl}\left(1-x_{rg}\right)m_{tot}\cdot\frac{N_{eng}}{120}-W_{fuel} \\ W_{rg} &= n_{cyl}x_{rg}m_{tot}\cdot\frac{N_{eng}}{120} \end{aligned} \quad . \tag{1}$$

Here, n_{cyl} is the number of cylinders, N_{eng} is the engine speed in RPM, and W_{fuel} is the mass flow rate of fuel injected into the cylinders. In addition, m_{tot} represents the total amount of mixture trapped in each cylinder at Intake Valve Closing (IVC) and can be calculated as

$$m_{tot} = \frac{p_{ivc}V_{ivc}}{RT_{ivc}} \tag{2}$$

where R is the universal gas constant. The cylinder volume at IVC, V_{ivc}, can be calculated as

$$\begin{aligned} V_{ivc} &= V\left(\theta_{ivc}\right) \\ &= V_0+\frac{\pi B_{cyl}^2}{4}\left(L_{cyl}+s_{cyl}-s_{cyl}\cos\left(\theta_{ivc}\right)\right. \\ &\qquad \left.-\sqrt{L_{cyl}^2-\left(s_{cyl}\sin\left(\theta_{ivc}\right)\right)^2}\right) \end{aligned} \tag{3}$$

where θ_{ivc} is the crank angle at IVC measured by the speed encoder, V_0 is the cylinder volume at Top Dead Center (TDC), L_{cyl} is the connecting rod length, B_{cyl} is the bore diameter, and s_{cyl} is half of the stroke length.

With the mass flow rates of the fresh charge and the residual gas estimated according to (1), the cylinder charge temperature at IVC, T_{ivc}, can then be obtained as

$$T_{ivc} = \left(1-x_{rg}\right)T_{fc}+x_{rg}T_{rg}\,, \tag{4}$$

where $(\cdot)_{fc}$ and $(\cdot)_{rg}$ denote the variables associated with the fresh charge and the residual gas, and T denotes the temperature of the mixture.

Due to the slowly varying offset and the noise in the in-cylinder pressure measurements, the measurements are adjusted by considering polytropic compression and expansion process [3]. Thus, the in-cylinder pressures during compression and expansion after both valves are closed can be fitted to equation (5).

$$pV^{\kappa_c}=C_1 \text{ and } pV^{\kappa_e}=C_2\,, \tag{5}$$

where C_1 and C_2 are constants, while κ_c and κ_e are the polytropic exponents of the compression and expansion strokes, respectively. Figure 2 illustrates the extracted

polytropic exponents for compression and expansion for various operation conditions with fuel E0 and E85.

After the in-cylinder pressures are adjusted, the cylinder pressures at IVC under different operation conditions can be estimated. As shown in Figure 3, the in-cylinder pressure at IVC, p_{ivc}, can be well approximated as an affine function of the cycle-average pressure in the intake manifold, p_{im}.

$$p_{ivc} = a_{1,p_{ivc}} p_{im} + a_{0,p_{ivc}} \tag{6}$$

Under the assumption of a polytropic compression, the in-cylinder pressure and temperature before combustion can be then obtained as

$$p_{bc} = p_{ivc}\left(\frac{V_{ivc}}{V_c}\right)^{\kappa_c} \text{ and } T_{bc} = T_{ivc}\left(\frac{V_{ivc}}{V_c}\right)^{\kappa_c - 1}. \tag{7}$$

where V_c denotes the cylinder volume at the combustion angle, θ_c.

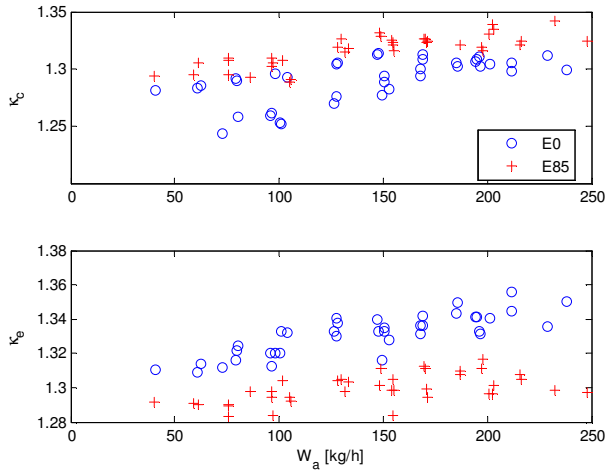

Figure 2: Modeled polytropic compression and expansion stroke using the measured in-cylinder pressures

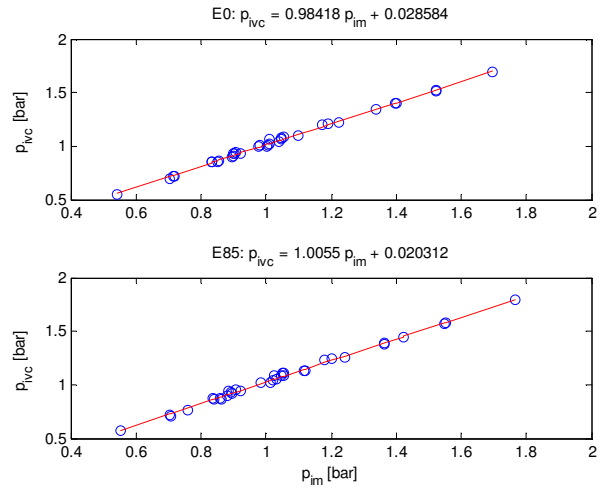

Figure 3: Modeled in-cylinder pressure at intake valve closing as a linear function of the intake manifold pressure

Instantaneous Combustion Heat Release

The heat release due to combustion is considered here to occur instantaneously at θ_c, which results in a sharp increase in the in-cylinder pressure and temperature after combustion.

$$p_{ac} = p_{bc} \cdot {}^{T_{ac}}\!/_{T_{bc}} \text{ and } T_{ac} = T_{bc} + \Delta T_{comb} \tag{8}$$

Under the assumption of instantaneous heat release, the combustion angle, θ_c, is thus the location of the peak pressure and can be computed as

$$\theta_c = \theta_{SOI} + \Delta\theta_c \tag{9}$$

where θ_{SoI} denotes the angle at the Start of Ignition (SoI), and $\Delta\theta_c$ denotes the burning duration. As presented in [4], the burning duration depends on engine speed, in-cylinder mixture air-to-fuel ratio, and EGR ratio. In a flex-fuel application, the burning duration is also a function of the ethanol concentration in the gasoline-ethanol fuels. In the current model, the burning duration is estimated directly from the in-cylinder pressure measurements and considered as an input.

As described in [5], the temperature increase ΔT_{comb} can be determined by

$$\Delta T_{comb} = \frac{m_{fuel} q_{HV} \eta_{comb}}{c_v m_{tot}} = \frac{(1 - x_r) q_{HV} \eta_{comb}}{c_v (\lambda \cdot AFR_s + 1)}, \tag{10}$$

where c_v is the specific heat capacity of the mixture at constant volume, and η_{comb} is the combustion efficiency. The combustion efficiency is computed as a function of the normalized air-to-fuel ratio, λ [5, 6].

$$\eta_{comb} = 0.95 \min(1, \quad 1.2\lambda - 0.2) \tag{11}$$

Here, q_{HV} and AFR_s denote the heat of combustion and stoichiometric air-to-fuel ratio, respectively. In order to model the engine behavior with ethanol fuels, these two fuel properties are modeled in (12) as functions of the volumetric ethanol content, *etoh*, based on the fuel properties of gasoline and ethanol in Table 1.

$$\begin{aligned} x &= \frac{\rho_{E0} \cdot etoh}{\rho_{E0} \cdot etoh + \rho_{E0} \cdot (100 - etoh)} \\ AFR_s &= (1 - x) \cdot AFR_{s,E0} + x \cdot AFR_{s,E100} \\ q_{HV} &= (1 - x) \cdot q_{HV,E0} + x \cdot q_{HV,E100} \end{aligned} \tag{12}$$

	Gasoline	Ethanol
Low Heating Value [MJ/kg]	42.4	26.8
Stoichiometric AFR	14.3	9.0
Density [g/cm^3]	0.74	0.79

Table 1: Fuel properties of gasoline and ethanol [7]

Polytropic Expansion

With the assumption of a polytropic expansion process, the pressure and temperature at Exhaust Valve Open (EVO) can be obtained as

$$p_{evo} = p_{ac}\left(\frac{V_c}{V_{evo}}\right)^{\kappa_e} \text{ and } T_{evo} = T_{ac}\left(\frac{V_c}{V_{evo}}\right)^{\kappa_e - 1}, \quad (13)$$

where V_{evo} is the cylinder volume at EVO as calculated according to (3).

Exhaust Blowdown

The temperature of the exhaust flow leaving the cylinder, after the exhaust valve opens, can be modeled as a quasi-adiabatic expansion of the gas down to the exhaust manifold pressure [2]

$$T_{bd} = T_{evo}\left(\frac{p_{em}}{p_{evo}}\right)^{\frac{\kappa_{bd}-1}{\kappa_{bd}}} + \Delta T_{bd}. \quad (14)$$

Here, κ_{bd} is the polytropic exponent during blowdown, and ΔT_{bd} captures the temperature difference between a pure adiabatic blowdown temperature and the actual measured temperature in the exhaust manifold.

VARIABLE VALVE TIMING

In addition to the use of throttle, variable valve timing is another way of controlling the amount of fresh charge drawn in by the engine. Compared with the conventional engines, the decoupling of camshaft and crankshaft permits the adaptation of intake and exhaust valve timing to a variety of engine speeds and cylinder charges. Variable valve timing enables the control of the amount of fresh air and residual gas trapped in the cylinders. Consequently, it improves the engine power output with favorable torque curves throughout a wide range of engine speeds. In fact, it also helps to reduce emissions, fuel consumption, and engine noise [8].

In order to improve the control of variable valve timing, various methods [9-11] have been developed in literature for modeling its effects on the amount of residual gas during internal exhaust gas recirculation. Without a direct measure of residual gas, the model proposed in [9] has been used to estimate the mass fraction of the burned residual gas x_{rg} in an iterative manner. The key element in this model is an energy balance at IVC

$$\left(c_{v,fc}m_{fc} + c_{v,rg}m_{rg}\right)T_{ivc} = c_{v,fc}m_{fc}T_{fc} + c_{v,rg}m_{rg}T_{rg}. \quad (15)$$

The total mass of mixture trapped in the cylinder at IVC, as expressed in (16), is a mixture of the fresh charge, burned residual gas, and fuel [9]

$$m_{tot} = m_{fc} + m_{rg} + m_{fuel}. \quad (16)$$

Given an initial estimate of the residual mass fraction x_{rg} and measurements of the fresh air charge m_{fc} and the amount of injected fuel m_{fuel}, then

$$m_{tot} = \frac{m_{fc} + m_{fuel}}{1 - x_{rg}^{old}}, \quad (17)$$

and the cylinder charge temperature at IVC, T_{ivc}, can be calculated according to the law of ideal gas.

$$T_{ivc} = \frac{p_{ivc}V_{ivc}}{Rm_{tot}} \quad (18)$$

We assume that the heat flux from the chamber walls to the fresh charge is partly compensated for the fuel evaporating process [9]. The fresh charge temperature can then be estimated from (19) using a polytropic compression from manifold to cylinder conditions. The temperature of the burned residual gas is estimated as the exhaust manifold temperature.

$$T_{fc} = T_{im}\left(\frac{p_{im}}{p_{ivc}}\right)^{\frac{1-\kappa_{fc}}{\kappa_{fc}}} \quad (19)$$

Thus, the new residual mass fraction can be estimated using the energy balance at IVC in (16).

$$x_{rg}^{new} = \frac{c_{v,fc}\left(T_{ivc} - T_{fc}\right)}{c_{v,rg}\left(T_{rg} - T_{ivc}\right) + c_{v,fc}\left(T_{ivc} - T_{fc}\right)} \quad (20)$$

In the iterative procedure (17)-(20), the value of residual mass fraction used in each iteration is updated following (21) to avoid convergence issues.

$$x_{rg}^{used} = x_{rg}^{old} + \frac{x_{rg}^{new} - x_{rg}^{old}}{2} \quad (21)$$

In order to avoid such an iterative loop in the real-time simulation, the physical model proposed in [10] is used instead with its coefficients parameterized using the values obtained from the model in (17)-(21). The amount of residual gas captured by this model is composed of two components: (i) the contribution due to the backflow of the burned gas from the exhaust port to the cylinder during the valve overlap period; and (ii) the trapper gas in the cylinder just before the start of the valve-overlap flow.

$$m_{rg} = \int_{\theta_{ivo}}^{\theta_{evc}} W_{bf}(\theta)d\theta + m_{ivo} \quad (22)$$

where W_{bf} is the mass flow rate of the burned gas drawn back into the engine from the exhaust port during the valve overlap period, while m_{ivo} is the mass trapped in the cylinder at Intake Valve Open (IVO). As described in [10], these two components can be well approximated as

$$x_{rg} = a_{1,x_{rg}}\left(\frac{p_{em}}{p_{im}}\right)^{\frac{\kappa+1}{2\kappa}}\left(\frac{OF}{N_{eng}}\right)\sqrt{\frac{|p_{em} - p_{im}|}{\rho_{fc}}} + a_{2,x_{rg}}\frac{1}{r_c}\left(\frac{p_{em}}{p_{im}}\right)^{\frac{1}{\kappa}}, \quad (23)$$

where ρ_{fc} is the density of the fresh charge, r_c is the engine compression ratio, and OF is the overlap factor. The overlap factor is defined as

$$OF = \frac{D_{iv}A_{iv} + D_{ev}A_{ev}}{V_d}, \quad (24)$$

where D_{iv} and D_{ev} are the inner seat diameters of the intake and exhaust valves, and V_d is the displacement volume of the engine. A_{iv} and A_{ev} are defined as

$$A_{iv} = \int_{\theta_{ivo}}^{L_{iv}=L_{ev}} L_{iv}(\theta)d\theta \text{ and } A_{ev} = \int_{L_{iv}=L_{ev}}^{\theta_{evc}} L_{ev}(\theta)d\theta, \quad (25)$$

where L_{iv} and L_{ev} are the intake and exhaust valve lifts. In this paper, *OF* is first calculated using the profile of the camshafts, based on which the coefficients, $a_{i,OF}$ for i = 0, 1, 2 in (26) can be estimated [10].

$$OF = \frac{L_{v,\max} D_v}{B_{cyl}^3}\left(a_{2,OF}\theta_o^2 + a_{1,OF}\theta_o + a_{0,OF}\right) \quad (26)$$

Here, $\theta_o = \theta_{evc} - \theta_{ivo}$ is the overlap angle, while $L_{v,max}$ and D_v are the maximum valve lift and the average valve seat diameter, respectively.

Due to the supercharging effects of a turbocharger, the intake manifold pressure in a turbocharged engine can be higher than the pressure in the exhaust manifold. Such boost effects can push the flow from the intake runner into the cylinders or even into the exhaust during the valve overlap period. In fact, such a phenomenon is known as the scavenging effects. Thus, coefficient $a_{1,xrg}$ will have a different value to capture such effects.

Figure 4 compares the residual mass fraction predicted by model A in (17)-(21) and model B in (23) that is implemented in the simulation model. In addition, Figure 5 illustrates the modeled mass flow rate of the fresh charge based on model B. In the remainder of this paper, the mean absolute error in (27) is used as a modeling accuracy index

$$MAE = \frac{1}{n}\sum_{t=1}^{n}\left|y(t) - y_e(t)\right|, \quad (27)$$

where y and y_e are the measured and modeled values for the target variable, and n is the number of samples.

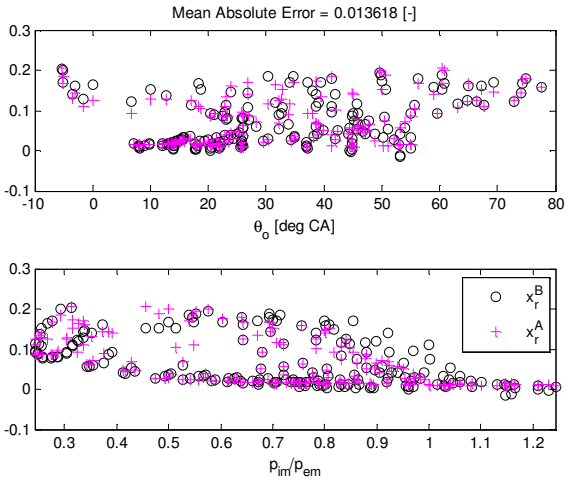

Figure 4: Residual mass fraction identified using model A in (17)-(21) and model B in (23)

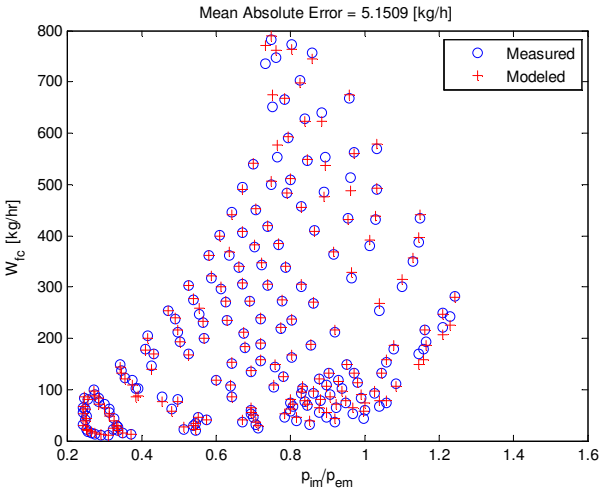

Figure 5: Modeled and measured mass flow rate of the fresh charge drawn from the intake port by the engine

TURBOCHARGER

The application of a turbocharger leads to increased cylinder charge and therefore increased power output. Among all the possible methods of super-charging an internal combustion engine, exhaust-gas turbocharging is most widely used because it can achieve high power output together with high engine efficiency, even on engines with low swept volumes [8]. Along with other advanced technologies such as direct fuel injection and variable valve timing, turbocharging has promoted the concept of engine downsizing to satisfy the increasing demands for fuel economy [12, 13].

The turbocharger model includes the modeling of a centrifugal compressor, a turbine, a wastegate, and a connecting shaft. All details are discussed below.

Compressor

The inlet air first acquires a high velocity from a rotating impeller and is then decelerated by a stationary diffuser before entering the intake system, which contributes to a pressure rise across a centrifugal compressor. Without accounting for the heat losses, the power, P_c, required to drive the compressor can be modeled from the first law of thermodynamics as follows [6]

$$P_c = \frac{1}{\eta_c} W_c \Delta h_c = \frac{1}{\eta_c} W_c c_p T_{up,c}\left(\left(\frac{p_{dn,c}}{p_{up,c}}\right)^{\frac{\kappa-1}{\kappa}} - 1\right), \quad (28)$$

where c_p and κ are the specific heat capacity under constant pressure and the adiabatic index of the air, Δh_c is the enthalpy change across the compressor, and W_c is mass air flow rate through the compressor. Here, the compressor efficiency, η_c, is introduced to account for the fact that the compression process is not isentropic.

Based on the performance map from the manufacturer, the efficiency of the compressor is modeled as a function of the pressure ratio across the compressor π_c, the

corrected rotational speed $N_{cor,c}$, and the corrected mass air flow rate $W_{cor,c}$ [14]. Figure 7 illustrates the computed compressor efficiencies using (29) for the experimental conditions considered. In the same figure, efficiencies from the manufacturer compressor map are also plotted. Please note the $V_{cor,c}$ in the figure is the corrected volumetric flow rate of the compressed air.

$$\eta_c = f\left(\frac{p_{dn,c}}{p_{up,c}},\quad N_{cor,c},\quad W_{cor,c}\right) \tag{29}$$

$$N_{cor,c} = N_{tc}\sqrt{\frac{T_{ref,c}}{T_{up,c}}},\ W_{cor,c} = W_c\sqrt{\frac{T_{ref,c}}{T_{up,c}}}$$

Here, $T_{ref,c}$ denotes the reference upstream temperature of the compressor used by the compressor manufacturer for its performance map.

In the ideal case when there are no heat losses, Δh_c can be estimated from Euler's equation for turbomachinery [14]. In a compressor with a radial-vane impeller, the ideal enthalpy across the compressor, $\Delta h_{ideal,c}$, can be expressed as

$$\Delta h_{ideal,c} = U_2 C_{\theta 2} - U_1 C_{\theta 1}. \tag{30}$$

As shown in Figure 6, point 1 is located on the impeller base near the entrance, while point 2 is located on its tip near the exit. Here, U_i is the impeller velocity at point i, $C_{\theta i}$ and C_{ri} are the tangential and radial velocity of air at point i, and h_i is the specific enthalpy of air at point i.

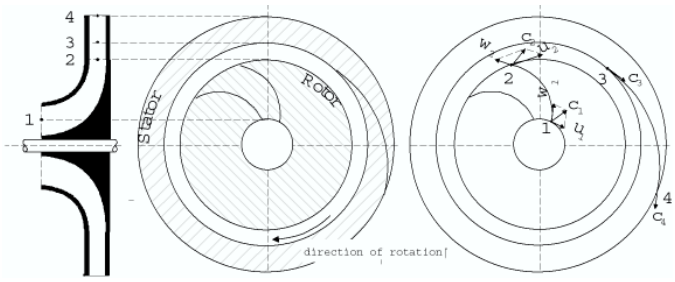

Figure 6: Schematic layout of a radial compressor with rotor (impeller) and stator (diffuser)

Under the assumption of no pre-whirl (i.e., $C_{\theta 1} = 0$), then

$$\Delta h_{ideal,c} = U_2 C_{\theta 2}. \tag{31}$$

If C_{r2} is parallel to the impeller vanes, then

$$C_{r2} = (U_2 - C_{\theta 2})\tan(\beta_c), \tag{32}$$

where β_c is back-sweep angle of the impeller blade.

According to the Bernoulli equation, the enthalpy at the impeller exit is given by

$$h_2 = h_4 - \frac{1}{2}\left(C_{r2}^2 + C_{\theta 2}^2\right). \tag{33}$$

The air density at the gap between the impeller and the diffuser can then be calculated as

$$\rho_2 = \rho_4\left(\frac{h_2}{h_4}\right)^{\frac{1}{\kappa-1}} = \rho_4\left(\frac{h_2}{c_p T_{dn,c}}\right)^{\frac{1}{\kappa-1}}, \tag{34}$$

and the mass air flow rate through the compressor is

$$W_c = A_{e,c} C_{r2} \rho_2, \tag{35}$$

where $A_{e,c}$ is the effective cross-section area between the impeller and the diffuser.

As expressed in equations (30)-(35), the model is able to predict the mass air flow rate through the compressor once the parameters β_c and $A_{e,c}$ are fitted based on the experimental data. In this paper, a nonlinear least square parameter estimation algorithm is used. Figure 8 shows the predicted values of the mass air flow rate through the compressor using the proposed model.

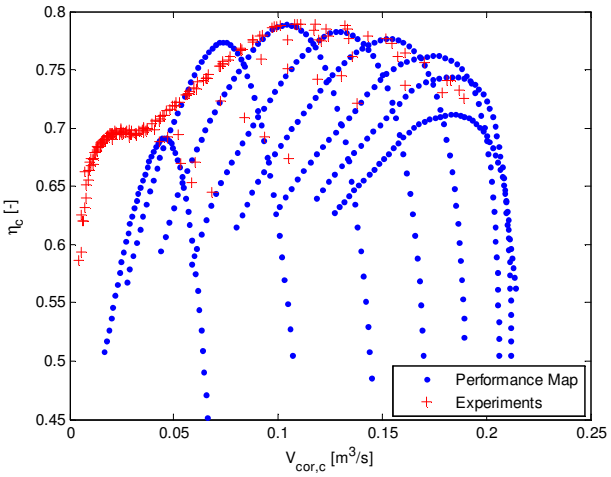

Figure 7: Compressor efficiency predicted using (29) that is fitted to the performance map

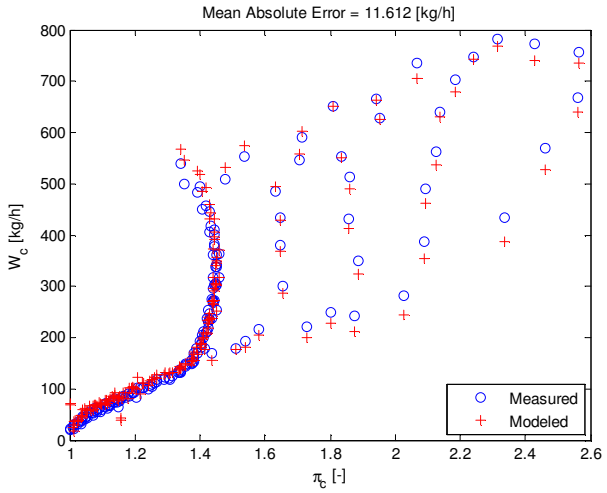

Figure 8: Modeled and measured mass air flow rate through the compressor using the model in (30)-(35)

Turbine + Wastegate

On the turbine side of a turbocharger, part of the exhaust gas exits through the turbine and drives the compressor

through the connecting shaft, while the rest leaves the exhaust manifold via the wastegate.

$$W_{eg} = W_t + W_{wg} = W_{fc} + W_{fuel} \tag{36}$$

Here, W_t and W_{wg} denote the mass air flow through the turbine and wastegate, and W_{eg} is the mass flow rate of exhaust gas expelled by the engine.

Similar to equation (28), the power, P_t, generated by the turbine can be modeled as

$$P_t = \eta_t W_t \Delta h_t = \eta_t W_t c_p T_{up,t} \left(1 - \left(\frac{p_{dn,t}}{p_{up,t}} \right)^{\frac{\kappa-1}{\kappa}} \right). \tag{37}$$

The turbine efficiency, η_t, typically has the shape of an inverted parabola for a fixed rotational speed, and thus can be modeled as a quadratic or cubic polynomial in the blade-speed ratio U/C, with its coefficients depending on the turbocharger speed N_{tc} [14, 16, 17].

$$\eta_t = f\left(\frac{U}{C}, \quad N_{cor,t} \right) \tag{38}$$

The blade-speed ratio, as defined in [14], is

$$\frac{U}{C} = \frac{\pi D N_{tc}}{60 \sqrt{2 c_p T_{up,t} \left(1 - \left(\frac{p_{dn,t}}{p_{up,t}} \right)^{\frac{\kappa-1}{\kappa}} \right)}}$$

and the corrected turbine speed $N_{cor,t}$ is

$$N_{cor,t} = N_{tc} \sqrt{\frac{T_{ref,t}}{T_{up,t}}}.$$

Here, $T_{ref,t}$ denotes the reference upstream temperature of the turbine in its performance map.

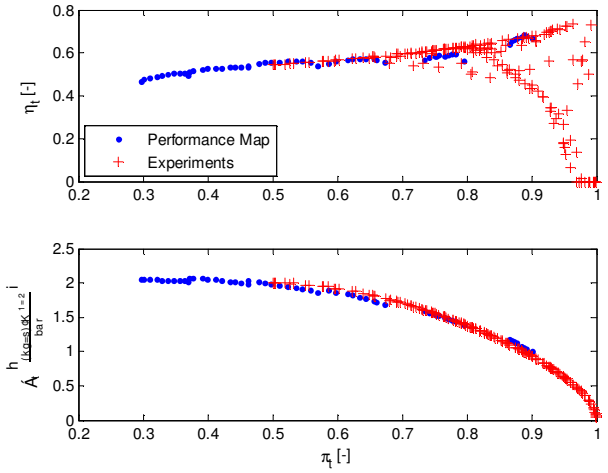

Figure 9: Turbine efficiency and flow parameter predicted for the turbine with models identified from the performance map

As described in [14], the turbine and wastegate can be modeled as a standard orifice model in (39) with varying cross-section areas. If p_{up} and p_{dn} are the upstream and downstream pressures of an orifice, the mass flow through the orifice, W, is given by

$$W = C_q A \frac{p_{up}}{\sqrt{R T_{up}}} \Phi \cdot \tag{39}$$

$$\Phi = \begin{cases} \sqrt{\frac{\kappa}{\kappa-1} \left(\left(\frac{p_{dn}}{p_{up}} \right)^{\frac{2}{\kappa}} - \left(\frac{p_{dn}}{p_{up}} \right)^{\frac{\kappa+1}{\kappa}} \right)} & \left(\frac{p_{dn}}{p_{up}} \right) > \left(\frac{2}{\kappa+1} \right)^{\frac{\kappa}{\kappa-1}} \\ \sqrt{\frac{\kappa}{\kappa-1}} \left(\frac{2}{\kappa+1} \right)^{\frac{1}{\kappa-1}} & \left(\frac{p_{dn}}{p_{up}} \right) \le \left(\frac{2}{\kappa+1} \right)^{\frac{\kappa}{\kappa-1}} \end{cases}$$

Here, Φ captures the restriction of flow to subsonic speeds, and C_qA, defined as the effective cross-section area A_e, is the product of the discharge coefficient and the opening of the orifice. In this study, the effective area of the turbine is modeled as a function of the turbine pressure ratio π_t, and the corrected turbine speed $N_{cor,t}$.

$$A_{e,t} = \frac{a_1}{\left(\frac{p_{dn,t}}{p_{up,t}} \right)} + a_0 \tag{40}$$

where the coefficients a_i are functions of the corrected turbine speed, i.e., $a_i = a_{1,i} N_{cor,t} + a_{0,i}$ for $i = 0, 1$. After models (38) and (40) are parameterized according to the turbine performance map using curve fitting techniques, the turbine efficiency and flow parameter, as illustrated in Figure 9, can be predicted for experimental conditions. The turbine flow parameter, as commonly used in the manufacturer's performance maps, is defined as

$$\phi_t = \frac{W_t \sqrt{T_{up,t}}}{p_{up,t}}. \tag{41}$$

Please note the predicted efficiency for the experimental conditions in Figure 9 drops to near-zero value when the pressure ratio across the turbine approaches to one. This is actually caused by the fact that the blade-speed ratio, based on which turbine efficiency is modeled, goes to infinity as its pressure ratio approaches to one.

The effective area of the wastegate depends on the angle of the valve that is controlled in a nonlinear manner by the duty-cycle d_{wg} and influenced by the downstream pressure of the compressor, and the pressure drop across the turbine. In this paper, a small-scale Radial Basis Neural Network (RBNN) in (42) is used to capture such nonlinearity. After the effective areas of the turbine and the wastegate are estimated, the mass flow rate of exhaust gas through them can be tracked separately. Consequently, the flow rate of the exhaust gas expelled from the engine, as illustrated in Figure 10, can then be estimated according to (36)

$$A_{e,wg} = f_{RBNN}\left(p_{dn,c}, \quad p_{up,t} - p_{dn,t}, \quad d_{wg} \right). \tag{42}$$

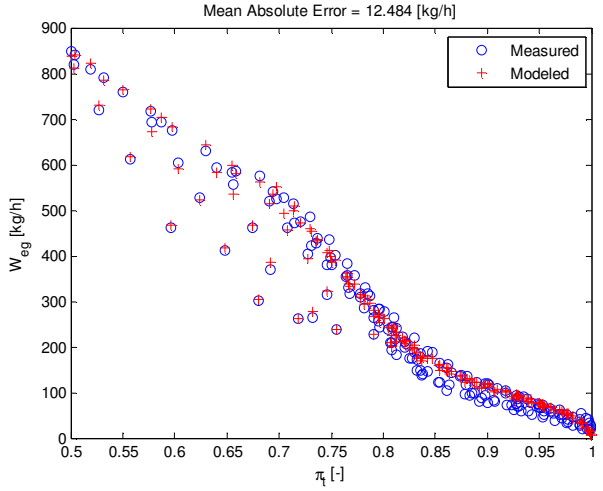

Figure 10: Modeled and measured mass flow rate of the exhaust gas that is expelled from the engine according to (36)

Shaft

The connecting shaft provides the power produced by the turbine to the compressor following Newton's law

$$I_{tc}\dot{N}_{tc} = \frac{1}{N_{tc}}\left(P_t - P_c\right), \text{ with } \dot{N}_{tc}(0) = \dot{N}_{0,tc} \tag{43}$$

where I_{tc} denotes the rotational inertia of the shaft, and $\dot{N}_{tc}$ is the acceleration of its rotational speed, N_{tc}.

THROTTLE

The flow through the throttle valve is represented by the standard orifice model with its cross-section area varying as a function of the throttle angle [6]. In this paper, a similar function as proposed in [18] is used to capture the relation between throttle angle θ_{th} and effective throttle opening $A_{e,th}$.

$$\begin{aligned} A_{e,th} &= A_{th}^1\left(1-\cos^2\left(a_2\theta_{th}^2 + a_1\theta_{th} + a_0\right)\right) + A_{th}^0 \\ \theta_{th} &= \left(\theta_{\max,th} - \theta_{\min,th}\right)\Theta_{th} + \theta_{\min,th} \end{aligned} \tag{44}$$

where Θ_{th} is relative position with respect to the lower mechanical stop of the throttle plate, $\theta_{min,th}$. Along with $\theta_{min,th}$, a_i for i = 0, 1, 2 are the fitting coefficients. After the effective throttle opening, $A_{e,th}$, computed using the experimental data according to the orifice model in (39), the coefficients in (44) can be fitted.

However, the standard orifice model in (39) becomes invalid when an engine is operated at the Wide-Open-Throttle (WOT) conditions. When the downstream and upstream pressures of the throttle are approximately the same, the mass air flow rate is then modeled as

$$W_{th} = \frac{p_{up,th}}{RT_{up,th}}V_{th}. \tag{45}$$

As illustrated in Figure 11, the volumetric flow speed of the air across the throttle at WOT conditions, V_{th}, has a linear correlation with the engine speed N_{eng}. In the same figure, the effective throttle area, $A_{e,th}$, plotted in blue circles are computed from the orifice model in (39), while those in the red line are calculated from (44). Figure 12 shows the modeled mass air flow rate passing through the throttle using the standard orifice model (39) and the volumetric flow model (45) at WOT conditions.

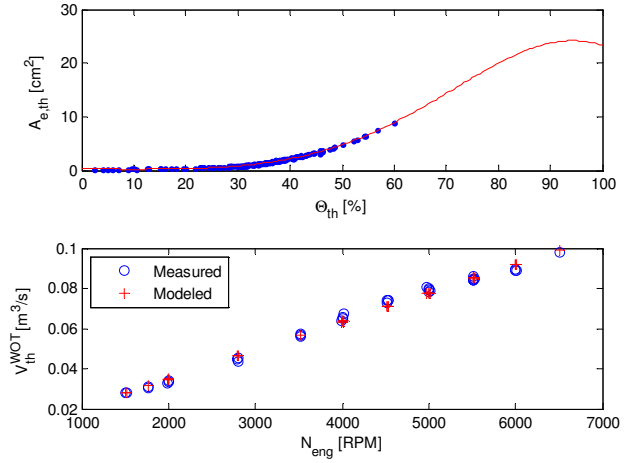

Figure 11: The effective cross-section area of the throttle and the volumetric air flow rate passing the throttle at WOT

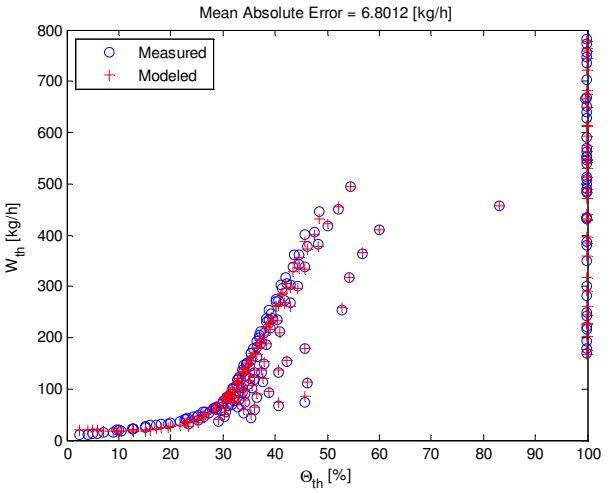

Figure 12: Modeled and measured mass flow rate via throttle

INTERCOOLER

The intercooler cools the compressed air towards a given coolant temperature, which helps to reduce knock in a SI engine. Without accounting for the pressure drop, the intercooler is modeled as a heat exchanger. Its outlet temperature, T_b, is given by

$$T_b = T_c - \eta_{ic}\left(T_c - T_{coolant}\right), \tag{46}$$

where T_c is the temperature of compressed air at the exit of the compressor, $T_{coolant}$ is coolant temperature, and η_{ic} is the efficiency of the intercooler. Following [18], the intercooler efficiency is modeled as

$$\eta_{ic} = a_0 + a_1 W_{ic} + a_2\left(\frac{T_c + T_{coolant}}{2}\right), \tag{47}$$

where W_{ic} is the flow rate of air passing the intercooler, and a_i for i = 0, 1, 2 are the fitting coefficients. Figure 13 shows the modeled and measured temperatures at the intercooler outlet along with its cooling efficiency.

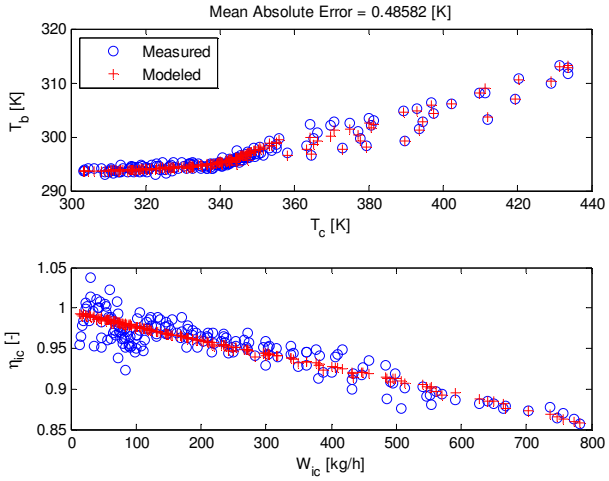

Figure 13: Modeled and measured intercooler outlet temperature and efficiency

EXHAUST BACK-PRESSURE DROP

After passing through the turbine, the exhaust gas exits the engine system and returns to the ambient air with a back-pressure drop. Under the assumption of laminar flow, this back-pressure drop is modeled as a function of its mass flow rate.

$$\begin{aligned}\Delta p &= p_{dn,t} - p_{amb} \\ &= a_0 + a_1 W_{eg} + a_2 W_{eg}^2\end{aligned}, \tag{48}$$

where p_{amb} denotes the ambient pressure. As shown in Figure 14, model (48) is able to capture the exhaust gas back-pressure drop with desirable accuracy.

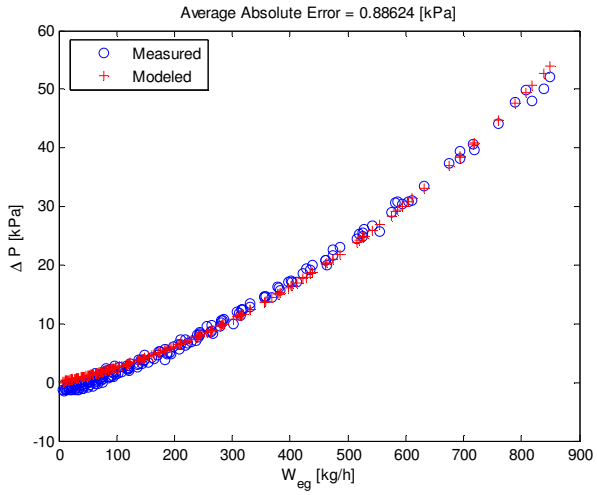

Figure 14: Modeled and measured intercooler outlet temperature and efficiency

MANIFOLDS

In the proposed model, three manifolds are employed to capture the filling and emptying dynamics in the engine system, including the induction volume, intake and exhaust manifolds. The dynamic behavior within each manifold is modeled as a chamber with fixed volume V using the state of mass, m, and pressure, p. Due to the significant temperature differences between the intake and exhaust path, different values are selected for the specific heat, c_v.

$$\begin{aligned}\frac{dm}{dt} &= \dot{m}_{in} - \dot{m}_{out} \\ \frac{dp}{dt} &= \frac{R}{c_v V}\left(\dot{H}_{in} - \dot{H}_{out}\right)\end{aligned}, \text{ and } T = \frac{pV}{mR} \tag{49}$$

with the initial conditions of

$$m(0) = m_0 = \frac{p_0 V}{RT_0}, \text{ and } p(0) = p_0$$

where $\dot{H}_{in}$ and $\dot{H}_{out}$ are the inlet and outlet enthalpy flow rate, $\dot{m}_{in}$ and $\dot{m}_{out}$ are the inlet and outlet mass flow rate.

INJECTOR

Different from a conventional port-fuel-injection engine, a gasoline direct-injection system injects the fuel directly into the combustion chamber at high pressures. Similar to a diesel engine, a proper mixture of the air and fuel is formed inside the cylinder. The application of direct fuel injection enables the combustion with a stratified fuel charge, which leads to improved fuel economy as well as reduced emission at low load [8].

As described in [6], the principle of a fuel injector is the same as a nozzle. Thus, the amount of fuel injected into the cylinder is determined by the injection duration, t_{inj}, and the mass flow rate of fuel through the injector that depends on the fuel rail pressure, p_{fuel}.

$$\begin{aligned}m_{fuel} &= W_{ref,fuel}\sqrt{\frac{p_{fuel}}{p_{ref,fuel}}}\left(t_{inj} - t_{d,inj}\right) \\ W_{fuel} &= n_{cyl} m_{fuel} \cdot \frac{N_{eng}}{120}\end{aligned} \tag{50}$$

where $t_{d,inj}$ is the injection delay time; $W_{ref,fuel}$ and $p_{ref,fuel}$ are the reference values for mass flow rate through the injector and its corresponding fuel rail pressure. Figure 15 shows the predicted mass flow rate of the injected fuel using model (50).

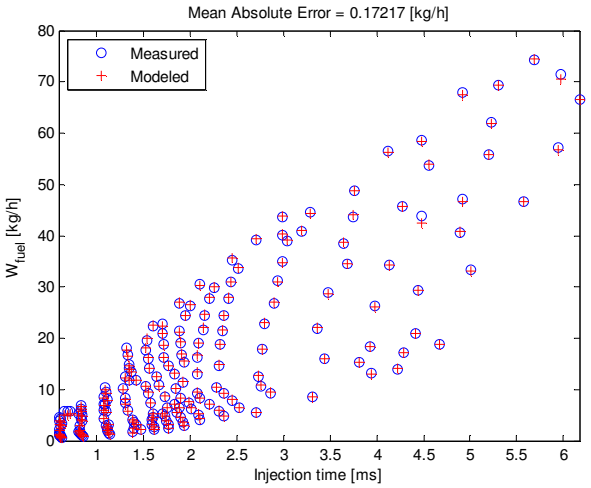

Figure 15: Modeled and measured mass flow rate of the injected fuel

EXPERIMENTAL DATA

The models presented above are parameterized using the experimental data that are collected from 2.0L four-cylinder turbocharged SIDI VVT engine. Various manifold locations, as indicated in Figure 16, were identified for the installation of pressure and thermocouples transducers. In addition, the engine is equipped with Kistler in-cylinder pressure transducers to enable the tracking of cylinder conditions, such as the in-cylinder pressure at IVC, and the polytropic exponents during the compression and expansion strokes.

The data used for model parameterization were collected when the engine was operated under steady operation conditions. During the dynamometer testing, the engine was operated from 800RPM up to 6500RPM with various control set-points for throttle angle, wastegate duty cycle, fuel injection and spark angle, variable valve timing, and fuel rail pressure. Moreover, transient engine data were also collected when the engine was subjected to step changes in the throttle angle at different speeds and loads. These data have been used for model validation.

SIMULATION

After the parameterized sub-models are implemented in Simulink using S-functions, a simulation model for the engine system, as illustrated in Figure 16, can then be established by linking them following the principles of mass and energy conservation. Table 2 lists the inputs and outputs of the engine model. Please note that the unit of *degCA* in Table 2 denotes the rotation angle of the crankshaft in degree.

Figure 17 - Figure 23 show the measured and simulated model outputs for two simulation cases, with which the transient behavior of the parameterized engine model is validated. In both cases, the engine was subjected to a step change in the throttle angle. In Case #1, the engine was operated around the engine speed of 2000RPM and intake air mass flow rate of 100kg/h without boost for fuel E0 and E85. In Case #2, the engine was boosted with gasoline (E0) at 30% duty cycle in wastegate around the engine speed of 3500RPM and intake air mass flow rate of 300kg/h.

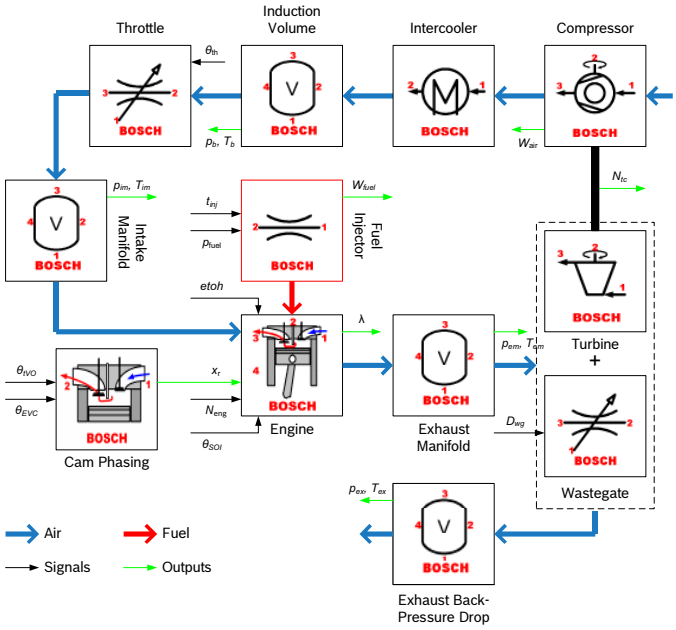

Figure 16: Block diagram of a control-oriented model

Inputs		
θ_{th}	degCA	throttle valve angle
θ_{IVO}	degCA	angle at intake valve open
θ_{EVC}	degCA	angle at exhaust valve closing
θ_{SOI}	degCA	angle at start of ignition
d_{wg}	%	wastegate duty cycle
N_{eng}	RPM	engine rotational speed
etoh	%	ethanol content
p_{fuel}	MPa	fuel rail pressure
t_{inj}	ms	fuel injection duration
Outputs		
p_b/T_b	bar/K	boost pressure
p_{im}/T_{im}	bar/K	intake manifold pressure/temperature
p_{em}/T_{em}	bar/K	exhaust manifold pressure/temperature
p_e/T_e	bar/K	exit pressure/temperature
W_{air}	kg/h	mass flow rate of intake air
W_{fuel}	kg/h	mass flow rate of injected fuel
N_{tc}	RPM	turbocharger rotational speed
λ	-	exhaust gas air/fuel ratio normalized with the stoichiometric value
x_{rg}	-	residual mass fraction

Table 2: List of input and output variables in the engine model

In both cases, the developed engine model is able to capture the transient dynamics in the intake air and injected fuel flow rate, the boost and intake manifold pressure, and the turbocharger rotational speeds when a step change in the throttle angle occurs. Compared with the experimental measurements, the presented model is able to estimate these outputs with desirable accuracy.

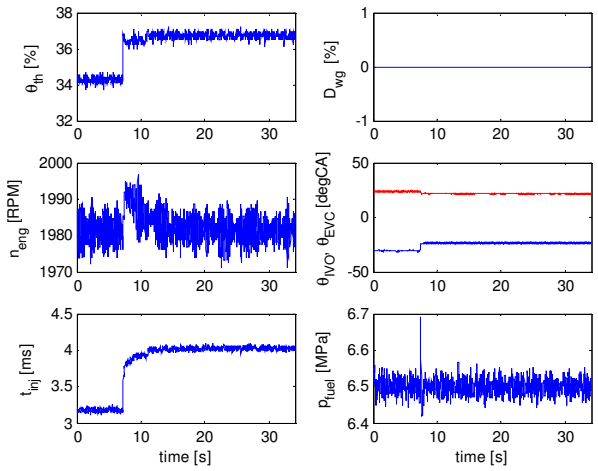

Figure 17: Engine operation conditions for CASE #1

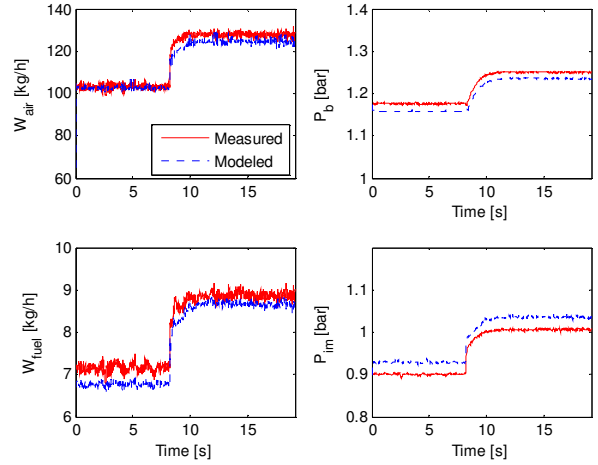

Figure 18: Simulated and measured outputs under operation conditions illustrated in Figure 17 with E0

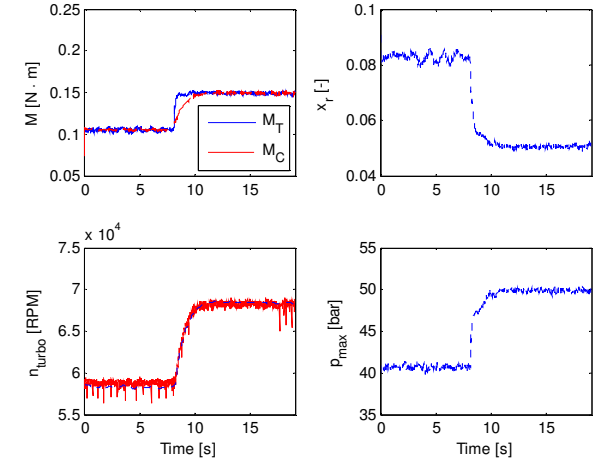

Figure 19: Simulated and measured outputs under operation conditions illustrated in Figure 17 with E0

Although the heating values of gasoline-ethanol fuel E85 are lower than that of gasoline, more fuel was injected into the combustion chamber to maintain a stoichiometric combustion. Due to the increased thermal efficiency of ethanol fuels, the in-cylinder peak pressures obtained from ethanol fuel E85 are higher than those from regular gasoline fuel (E0) in Figure 19 and Figure 21, thus indicating higher engine power outputs.

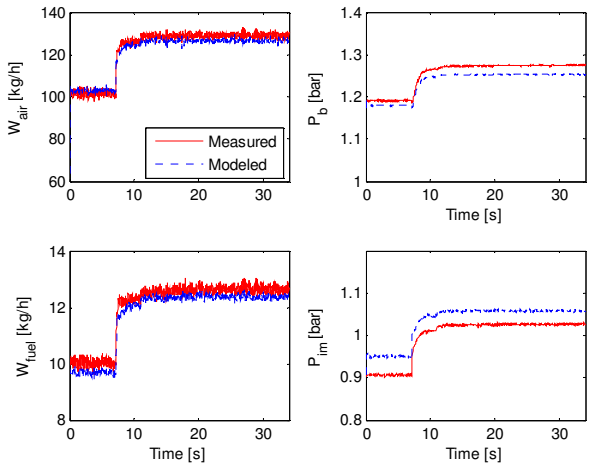

Figure 20: Simulated and measured outputs under operation conditions illustrated in Figure 17 with E85

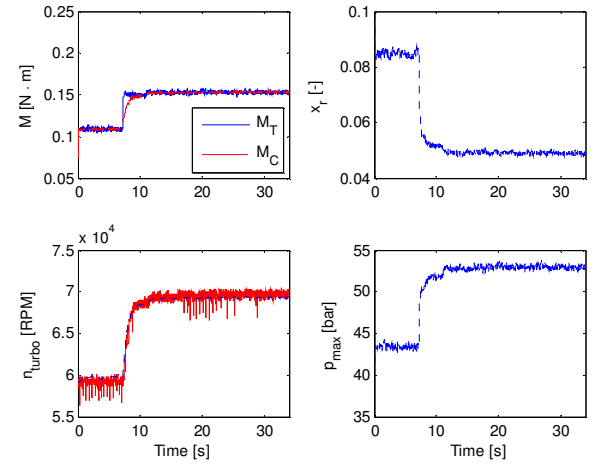

Figure 21: Simulated and measured outputs under operation conditions illustrated in Figure 17 with E85

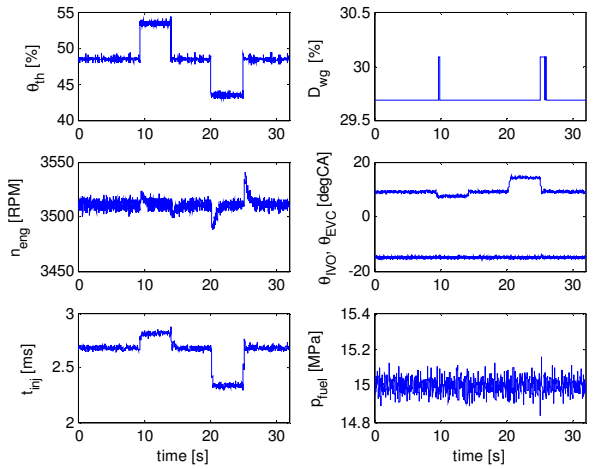

Figure 22: Engine operation conditions for CASE #2

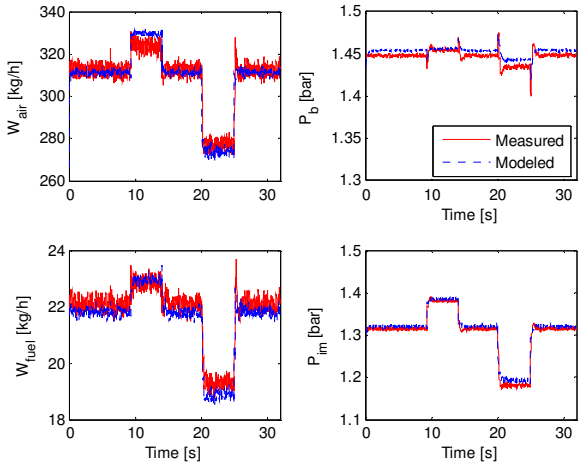

Figure 23: Simulated and measured outputs under operation conditions illustrated in Figure 22 with E0

CONCLUSION

In this paper, a control-oriented model was presented for a turbocharged Spark Ignition Direct Injection (SIDI) engine with Variable Valve Timing (VVT). The proposed model systematically integrates the models for different components including turbocharger, throttle, intercooler, fuel injector with those for variable valve timing effects and engine combustion behaviors. In order to investigate its modeling capability for flex-fuel applications, those fuel-dependent engine parameters are also identified. The development of such a model enables the simulation of engine performance with gasoline-ethanol fuels and the investigation of the effects of variable valve timing as well as boosting via the control of wastegate.

In this study, a four-cylinder turbocharged SIDI VVT was employed for dynamometer testing. In order to collect sufficient data for model parameterization, the engine was run from 800RPM up to 6500RPM with different control set-points for throttle angle, wastegate duty cycle, injection and spark angle, as well as fuel rail pressure. After the model was parameterized with the experimental data, its dynamic performance was validated using the transient engine data that were collected when the engine was subjected to step changes in the throttle angle. In both boosted and unboosted conditions, the model has demonstrated its capability in capturing the effects of variable valve timing and turbocharger boosting via the wastegate. In addition, the model has shown its potential in capturing the effects introduced by the gasoline-ethanol fuel blends.

ACKNOWLEDGMENTS

The present work has been performed within the scope of the “Optimally Controlled Flexible Fuel Powertrain Systems” project, sponsored by Department of Energy (DoE). The authors would like to acknowledge Michael Caruso at Robert Bosch LLC for his assistance in project administration as well as Nick Fortino and Mark Christie at Ricardo, Inc. for their support in dynamometer testing.

REFERENCES

1. D. Rausen. A dynamic low order model of homogenous charge compression ignition engines. *Master thesis*, University of Michigan, 2003
2. D. Rausen, A. Stefanopoulou, J. Kang, J. Eng, T. Kuo. A mean-value model for control of homogenous charge compression ignition (HCCI) engines. *Journal of Dynamic Systems, Measurement and Control*, vol. 127, pp. 355-62, 2005
3. P. Öberg and L. Eriksson. Control oriented modeling of the gas exchange process in variable cam timing engines. *SAE Technical Paper* 2006-01-0660
4. S.D. Hines, R.J. Tabaczunski, and J.M. Novak. The prediction for ignition delay and combustion intervals for a homogeneous charge, spark ignition engine. *SAE Technical Paper* 780232, 1978
5. L. Eriksson and I. Andersson. An analytical model for cylinder pressure in a four stroke SI engine. *SAE Tehcnical Paper* 2002-01-0371
6. J. Heywood. *Internal Combustion Engine Fundamentals*. McGraw-Hill series in mechanical engineering. McGraw-Hill, 1992
7. K. Nakata, S. Utsumi, A. Ota, K. Kawatake, T. Kawai, T. Tsunooka. The Effect of Ethanol Fuel on a Spark Ignition Engine, *SAE Technical Paper* 2006-01-3380
8. *Bosch Gasoline-Engine Management*, Robert Bosch Gmbh, 2nd edition, 2004
9. M. Mladek and C. Onder. A model for the estimation of inducted air mass and the residual gas fraction using cylinder pressure measurements. *SAE Technical Paper* 2000-01-0958
10. W. Jonathan, K. Wai, and J. Heywood. A model for predicting residual gas fraction in spark-ignition engines. *SAE Technical Paper* 931025
11. F. Ponti, J. Pianai, R. Suglia. Residual gas model for on-line estimation for inlet and exhaust continuous VVT engine configuration. In proceedings of *IFAC World Congress*, 2004
12. J. Strokes, R. Osborne, and T. Lake. A gasoline engine concept for improved fuel economy – the lean boost system. *SAE Technical Paper* 2000-01-2902
13. T. Lake. Turbocharging concepts for downsizing DI gasoline engines. *SAE Technical Paper* 2004-01-0036
14. P. Moraal and I. Kolmanovsky. Turbocharger modeling for automotive control application. *SAE Technical Paper* 1999-01-0908
15. N. Watson. Dynamic turbocharged diesel engine simulator for electronic control system development. *Journal of Dynamic Systems, Measurement, and Control*, vol. 106, pp. 27-45, 1998
16. J. Jensen, A. Kristensen, S. Sorenson, N. Houbak, E. Hendricks. Mean value modeling of a small turbo-charged diesel engine. *SAE* Technical Paper 910070

17. M. Mueller. Mean value modeling of turbocharged spark ignition engines. *Master's Thesis*, DTU, Denmark, 1997
18. L. Eriksson, L. Nielsen, J. Brugård, J. Bergström, F. Pettersson, and P. Andersson. Modeling of a turbocharged SI engine, *Annual Reviews in Control*, vol. 26, pp. 129-137, 2002

DEFINITIONS, ACRONYMS, ABBREVIATIONS

DI: Direct Injection

IVC: Intake Valve Closing

EVO: Exhaust Valve Open

RPM: Revolution Per Minute

TDC: Top Dead Center

VVT: Variable Valve Timing

SoI: Start of Ignition

SIDI: Spark Ignition Direct Injection